










Control of cortical slow oscillations and epileptiform discharges with photoswitchable type 1 muscarinic ligands

Jose M. Sanchez-Sanchez ^a, Fabio Riefolo ^b, Almudena Barbero-Castillo ^a, Rosalba Sortino^c, Luca Agnetta^d, Arnau Manasanch ^{a,e}, Carlo Matera ^{c,f}, Miquel Bosch ^{a,c}, Marta Forcella ^c, Michael Decker ^d, Pau Gorostiza^{c,g,h,*} and Maria V. Sanchez-Vives ^{a,h,*}

^aSystems Neuroscience, Institute of Biomedical Research August Pi i Sunyer (IDIBAPS), Barcelona 08036, Spain

^bTeamit Institute, Partnerships, Barcelona Health Hub, Barcelona 08025, Spain

^cInstitute for Bioengineering of Catalonia (IBEC), Barcelona Institute of Science and Technology, Barcelona 08028, Spain

^dInstitute of Pharmacy and Food Chemistry, University of Würzburg, Würzburg 97074, Germany

^eFaculty of Medicine and Health Sciences, University of Barcelona, Barcelona 08036, Spain

^fDepartment of Pharmaceutical Sciences, University of Milan, Milan 20133, Italy

^gCIBER-BBN, Madrid 28029, Spain

^hICREA, Barcelona 08010, Spain

*To whom correspondence should be addressed: Email: msanche3@recerca.clinic.cat (M.V.S.-V.); Email: pau@icrea.cat (P.G.)

Edited By Eric Klann

Abstract

Acetylcholine and the cholinergic system are crucial to brain function, including functions such as consciousness and cognition. Dysregulation of this system is implicated in the pathophysiology of neurological conditions such as Alzheimer's disease. For this reason, cholinergic neuromodulation is relevant in both basic neuroscience and clinical neurology. In this study, we used photopharmacology to modulate neuronal activity using the novel selective type-1 muscarinic (M_1) photoswitchable drugs: the agonist benzyl quinolone carboxylic acid-azopyperoxo (BAI) and the antagonist cryptozepine-2. Our aim was to investigate the control over these cholinergic receptors using light and to investigate the effects of these drugs on physiological spontaneous slow waves and on epileptic activity in the cerebral cortex. First, we used transfected HEK cell cultures and demonstrated BAI's preferential activation of M_1 muscarinic acetylcholine receptors (mAChRs) compared with M_2 mAChRs. Next, we found that white-light illumination of BAI increased the frequency of spontaneous slow-wave activity in brain cortical networks of both active slices and anesthetized mice, through M_1 -mAChRs activation. Illumination of cryptozepine-2 with UV light effectively suppressed not only the muscarinic-induced increase in slow-wave frequency, but also muscarinic-induced epileptiform discharges. These findings not only shed light on the role of M_1 acetylcholine receptors in the cortical network dynamics but also lay the groundwork for developing advanced light-based pharmacological therapies. Photopharmacology offers the potential for high-precision spatiotemporal control of brain networks with high pharmacological specificity in both healthy and pathological conditions.

Keywords: slow oscillations, epilepsy, photopharmacology, neuromodulation, acetylcholine

Significance Statement

The cholinergic system, linked to memory and cognition in the cortex, is implicated in neurological disorders. We investigated two novel cholinergic photoswitchable drugs, an agonist and an antagonist of M_1 -muscarinic receptors, to modulate cortical activity. First, in cell cultures, we demonstrated preferential activation of the agonist over M_1 receptors. Photoswitchable drugs can be activated by light, allowing spatiotemporal control of their action. Illumination of the M_1 -agonist BAI increased cortical slow-wave frequency in vitro and in vivo, revealing M_1 -muscarinic receptors' role in cortical rhythmicity. The novel M_1 -antagonist cryptozepine-2 not only blocked cholinergic effects on slow waves, it also blocked epileptiform discharges following illumination. These new insights into neuromodulation of complex emergent activity open possibilities for clinical translation.

Competing Interest: The authors declare no competing interests.

Received: July 16, 2024. **Accepted:** January 2, 2025

© The Author(s) 2025. Published by Oxford University Press on behalf of National Academy of Sciences. This is an Open Access article distributed under the terms of the Creative Commons Attribution-NonCommercial License (<https://creativecommons.org/licenses/by-nc/4.0/>), which permits non-commercial re-use, distribution, and reproduction in any medium, provided the original work is properly cited. For commercial re-use, please contact reprints@oup.com for reprints and translation rights for reprints. All other permissions can be obtained through our RightsLink service via the Permissions link on the article page on our site—for further information please contact journals.permissions@oup.com.

Introduction

The human brain supports our interactions with the outside world, encompassing sensorimotor actions to higher cognitive processes (1). Brain diseases can have a large impact on these interactions, affecting not only our ability to relate to the external world but also fundamental aspects of human identity, such as memories, cognition, and social interactions. With the high prevalence of neurological diseases and their significant societal impact, there is a critical need for innovative tools that enable noninvasive and precise modulation of neuronal activity, often referred to as neurotechnology. One such promising approach is photopharmacology, a multidisciplinary field that combines pharmacology, chemistry, and optics to design drugs that can be controlled using light, providing remote control over drug action without requiring genetic manipulation (2).

The cholinergic neuromodulation system plays a crucial role in the brain, not only in regulating transitions between different brain states (3, 4), as in wakening (5), but also in processes such as attention and memory (6). Dysfunction of the cholinergic system has been implicated in various brain pathologies, including Alzheimer's disease (7). In particular, cholinergic signaling in the cerebral cortex primarily occurs through muscarinic receptors (mAChRs), which are involved in a wide range of critical functions (for a review, see Brown (8)). While the structure and intracellular pathways of different mAChR subtypes in the brain neocortex, such as M_1 , M_2 , and M_4 (9, 10), have been extensively studied, their specific contributions to cortical network dynamics remain poorly understood. In this study, we aimed to further disentangle the M_1 mAChRs function in cortical dynamics using selective light-operated drugs.

We focused on cortical slow oscillations (SO), a prominent activity known to dominate cortical network activity during slow-wave sleep, deep anesthesia, and certain brain lesions (11–14). Photoswitchable molecules have already been demonstrated to photocontrol SO through the photoswitchable M_2 mAChR agonist, phthalimide-azo-iperoxo (PAI) (15, 16). In this study, we specifically examined how a photoswitchable M_1 mAChR agonist, benzyl quinolone carboxylic acid-azo-iperoxo (BAI) (17), affects cortical dynamics during SO in vitro and in vivo. Furthermore, we investigated the effects of a novel M_1 mAChR antagonist, cryptozepine-2 (cryptozepine for simplicity) (18), on SO and muscarinic-induced seizure-like activity in the cerebral cortex in vitro.

In summary, we confirmed cholinergic neuromodulation of SO and its involvement in cortical dynamics with a focus on M_1 mAChRs. We aimed to investigate the validity of using two novel photoswitchable drugs on cortical dynamics as a new method for investigating cholinergic mechanisms in large networks. The results of this research provide insights into the role of M_1 mAChRs in cortical function and demonstrate the potential of photopharmacology in modulating neuronal activity. Ultimately, these findings may contribute to the development of innovative therapeutic approaches for brain diseases involving the cholinergic system.

Results

BAI as a photoswitchable M_1 -muscarinic acetylcholine receptor agonist in HEK cells

To study cell responses to photopharmacological stimulation with BAI, we performed a real-time calcium imaging assay under continuous illumination (one-photon excitation [1PE]) in HEK cells transiently transfected with M_1 mAChRs and loaded with the

fluorescent calcium indicator Oregon Green BAPTA-1 AM (OGB-1 AM). Neither the application of the vehicle (Fig. 1b and c, gray bar, and Fig. 1d) nor the illumination alone evoked calcium responses (control experiments). Calcium oscillations characteristic of M_1 mAChR activation (predominantly G_q -coupled) were observed upon application of *trans*-BAI (orange bar, active isomer, dark-adapted state) and were terminated by photoconversion to *cis*-BAI (inactive isomer) under 365-nm illumination. Subsequent *cis* to *trans* isomerization under 460-nm light rapidly reactivated M_1 mAChRs, triggering oscillatory calcium responses that are shown as both representative traces of individual cells (Fig. 1b) and average of individual cell responses (Fig. 1c). The agonist acetylcholine (ACh) was applied in each experiment as a positive control (green bar).

The quantification of the response showed that *trans*-BAI, like ACh, significantly stimulated the release of intracellular calcium, while illumination with 365 nm (*trans* to *cis*) decreased calcium responses by 46% (from $80 \pm 8\%$ during *trans*-BAI to $34 \pm 5\%$ during *cis*-BAI, $P = 0.000014$), (Fig. 1d, $n = 53$ cells from four independent experiments). However, we noted that the responses triggered by BAI in the dark were greater compared with those under 460-nm illumination, possibly due to only partial photoisomerization of the compound (higher *trans* content in fully relaxed BAI in the dark). Additionally, we measured BAI-mediated calcium responses in HEK cells co-expressing M_2 mAChRs and G_{qTOP} (the latter transduces $G_{i/o}$ -mediated receptor activation to calcium responses for the sake of comparison) (19) in order to study the selectivity of BAI for M_1 vs. M_2 mAChRs. In cells expressing M_1 mAChRs, the photoconversion of BAI from *cis* to *trans* induced a stronger activation of calcium responses compared with the M_2 mAChR-expressing cells for all the concentrations tested (Fig. 1e), demonstrating a preference of BAI for M_1 vs. M_2 mAChRs with a maximal difference at $1 \mu\text{M}$ ($80 \pm 58\%$ on M_1 cells, $n = 45$, over $39 \pm 33\%$ on M_2 cells, $n = 61$, $P = 0.000031$). Moreover, the effectiveness of BAI in activating M_1 mAChRs significantly increases with the dosage, while its activation of M_2 mAChRs is weakly dose dependent (Fig. S1). Furthermore, photoresponses were absent in cells not expressing M_1 or M_2 - G_{qTOP} mAChRs (Fig. S2; control). Explanation of the F/F_0 calculation is described in the Materials and methods section.

Dose-dependent effects of BAI isomers on cortical activity

Cerebral cortex slices in vitro express spontaneous rhythmic network activity as SO (Fig. 2a) (11, 20). This is a rhythmic activity equivalent to that generated in the cortex in vivo during slow-wave sleep and deep anesthesia (21, 22) and is an emergent activity of the cortical network that results from the integration of cellular and synaptic properties. These oscillations consist of periods of activity or Up states interspersed with periods of silence or Down states (11, 23) (Fig. 2a).

To identify the most suitable range of drug concentrations to achieve a robust modulation of SO by light, we generated a dose-response curve under the effect of *cis*- and *trans*-BAI isomers in cortical slices in vitro. The baseline characterized by SO was recorded as control. Then, three different concentrations of *trans*- and *cis*-BAI were applied to the bath (1, 2, and $3 \mu\text{M}$, $n = 4$ slices, for both *trans*- and *cis*-BAI isomers; Fig. 2b).

Compared with the control condition, the *trans*-BAI bath application led to an increase in oscillatory frequency with a reduction in Down-state duration, with the maximum effect at $3 \mu\text{M}$ (from 0.4 ± 0.08 Hz during control to 0.92 ± 0.05 Hz during $3 \mu\text{M}$

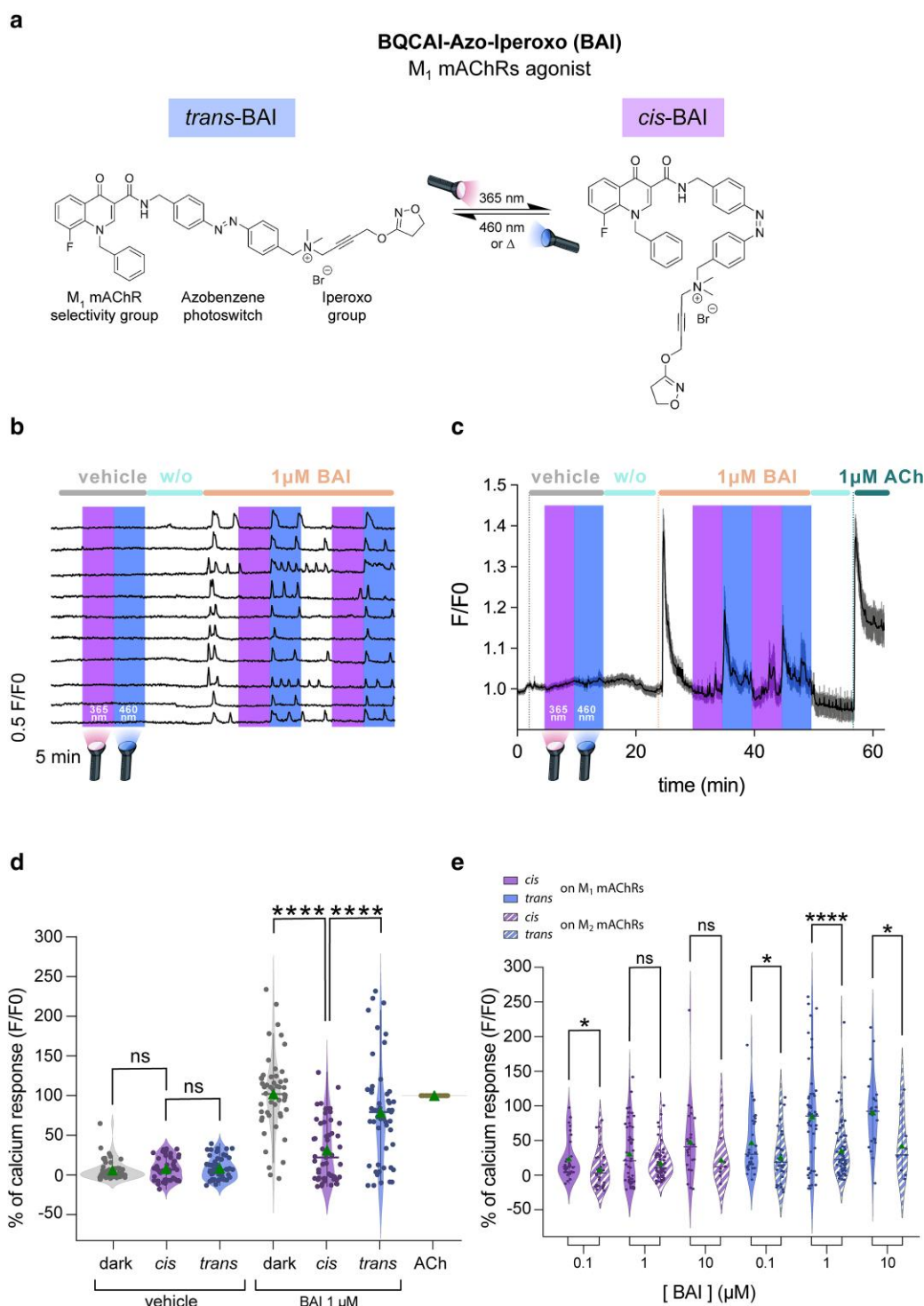


Fig. 1. In vitro pharmacological characterization of BAI in HEK cells. **a)** Chemical structures of the *cis*- and *trans*-isomers of BAI, along with the wavelengths required for their photoswitching. **b)** Real-time calcium imaging traces from individual HEK cells transiently transfected with human M₁ mAChRs. Traces show intracellular calcium activity under continuous illumination with 365-nm (*trans*-to-*cis*) and 460-nm (*cis*-to-*trans*) light. Responses to the vehicle (gray bar) and BAI (1 μ M, orange bar) are depicted. Light blue bars represent wash-out periods, while acetylcholine (ACh, green bar, 1 μ M) is used as a positive control. **c)** Intracellular calcium responses ($n = 15$ cells) to 1 μ M BAI under 365- and 460-nm illumination, demonstrating oscillatory calcium responses triggered by *trans*-BAI and reduced by *cis*-BAI. ACh application also triggers calcium responses, serving as a control for M₁ mAChR activation (100% of calcium response). **d)** Violin plots with individual data points per cell displaying the quantified calcium responses to *trans*-BAI and *cis*-BAI in HEK cells expressing M₁ mAChRs. *Trans*-BAI significantly increased intracellular calcium levels, while *cis*-BAI reduced calcium responses by 46% (from $80 \pm 8\%$ during *trans*-BAI to $34 \pm 5\%$ during *cis*-BAI, $n = 53$, $P = 0.000014$, Tukey's post-hoc test). Vehicle application and illumination alone did not evoke any calcium responses (control experiments). **e)** Comparison of calcium responses in HEK cells co-expressing either M₁ mAChRs or M₂ mAChRs, alongside G_qTOP (a reporter for G_{i/o}-mediated calcium signaling) at different BAI concentrations (0.1, 1, and 10 μ M). BAI showed a clear preference for M₁ mAChRs over M₂ mAChRs, with a maximum difference at 1 μ M ($80 \pm 58\%$ on M₁ cells, $n = 45$, over $39.67 \pm 33.41\%$ on M₂ cells, $n = 61$, $P = 0.000031$, Welch's test). Data are presented as means \pm SD; P-values: * ≤ 0.05 ; **** ≤ 0.0001 ; ns = not significant.

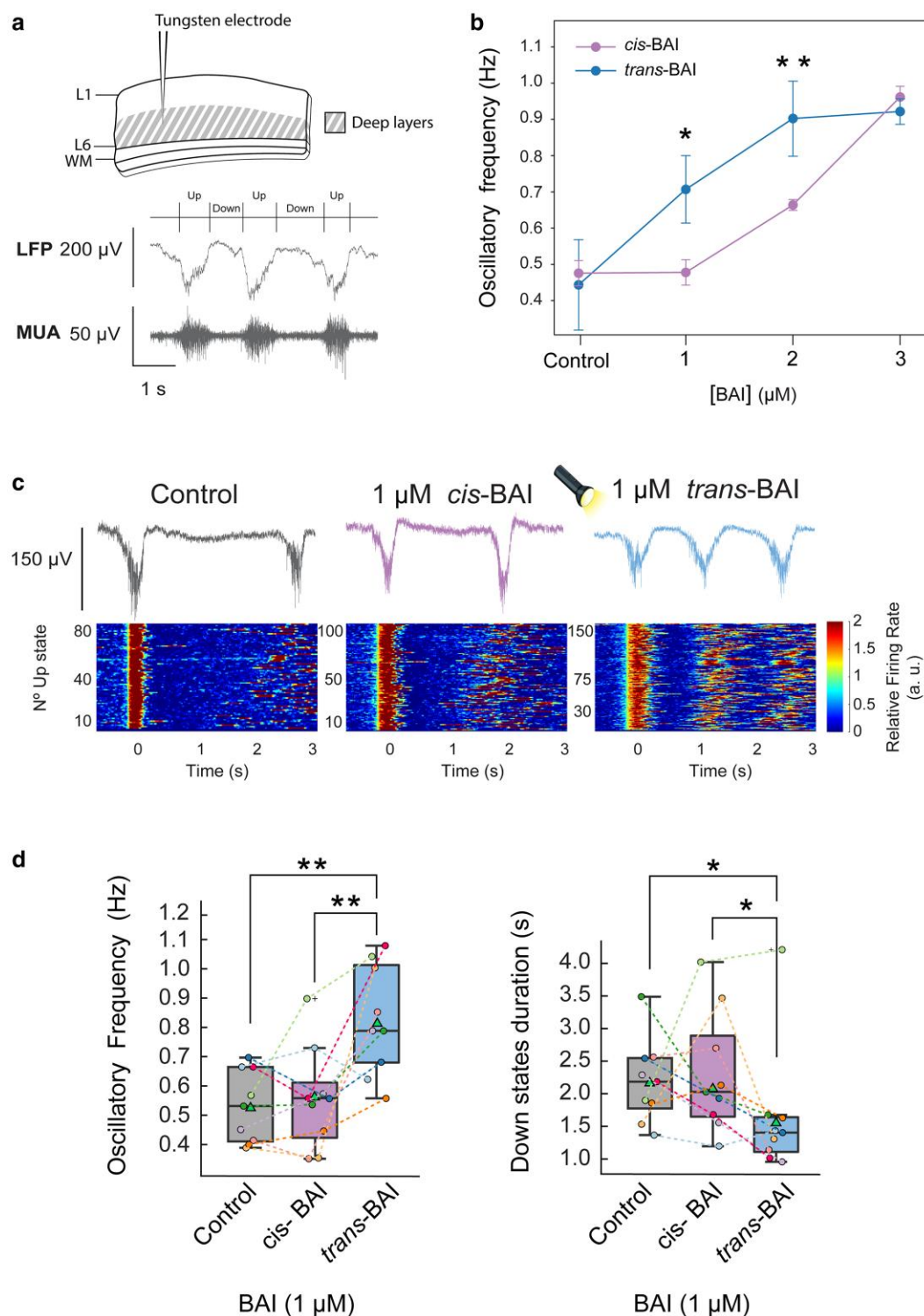


Fig. 2. Dose-dependent modulation of cortical SO by BAI isomers and light-induced photocontrol in vitro. **a**) Schematic diagram of the experimental setup used for cortical slice recordings (top). The LFP traces display spontaneous SO, distinguishing Up states (periods of activity) and Down states (periods of silence) (middle). MUA associated with these oscillations is shown at the bottom. **b**) Dose-response effects of *cis*- and *trans*-BAI on oscillatory frequency (Hz) in brain slices ($n=4$ for each isomer) at three concentrations: 1, 2, and 3 μ M. Significant differences between *cis*- and *trans*-BAI were observed at 1 μ M ($P=0.0317$) and 2 μ M ($P=0.0079$). **c**) Representative LFP traces (top) and raster plot of relative FR (bottom) from a ferret brain slice under control conditions, following application of 1 μ M *cis*-BAI (preilluminated at 365 nm to maintain the *cis* form), and after photoconversion to *trans*-BAI via white-light illumination. **d**) Boxplots with individual data points representing the median values (black line) and mean values (green triangles) of oscillatory Hz and Down-state duration (s) under the control condition, after *cis*-BAI application, and following photoconversion to *trans*-BAI. The oscillatory frequency under 1 μ M *cis*-BAI showed no significant change from control (0.53 ± 0.11 Hz during control to 0.55 ± 0.16 Hz, $n=9$ brain slices, $P=0.920$). Upon photoconversion to *trans*-BAI, the oscillatory frequency significantly increased (from 0.53 ± 0.11 to 0.83 ± 0.06 Hz, $P=0.003$). Down-state duration decreased significantly after photoconversion (from 2.19 ± 0.60 s during control to 1.64 ± 0.93 s, $P=0.034$). Data are presented as means \pm SD; P-values: * ≤ 0.05 ; ** ≤ 0.01 ; ns = not significant. Statistical analysis was performed using the two-sided Mann-Whitney U test.

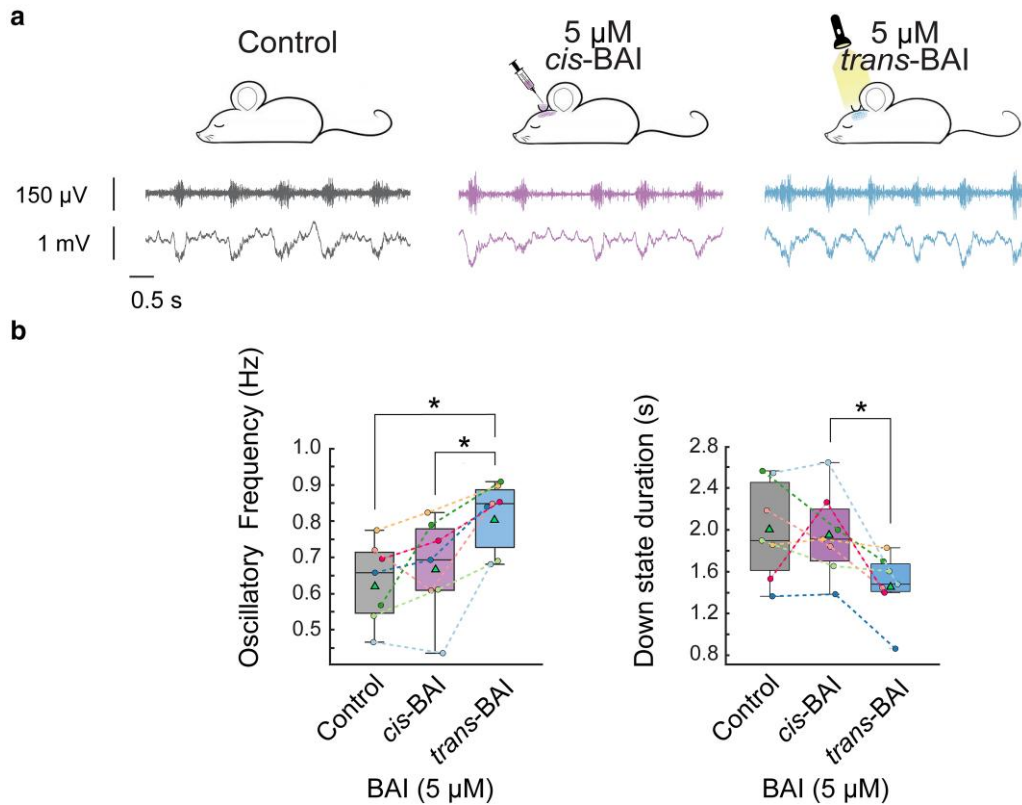


Fig. 3. Photocontrol of SO with BAI and direct illumination with white light in vivo. a) Diagram of the in vivo photocontrol protocol (top). Representative MUA traces (middle) and LFP traces (bottom) recorded from the primary visual cortex (V1) of anesthetized mice under three conditions: control (anesthetized), following the topical application of 5 μ M *cis*-BAI (preilluminated with 365 nm light) on the cortex, and after photoconversion to *trans*-BAI via white-light illumination of the brain. b) Boxplots with individual data points representing the median values (black line) and mean values (green triangles) of oscillatory frequency (Hz) and Down-state duration (s) under control conditions, after *cis*-BAI application, and following photoconversion to *trans*-BAI. Compared with the control, *cis*-BAI application did not significantly alter the oscillatory frequency (0.63 ± 0.10 to 0.67 ± 0.12 Hz, $n = 7$ mice, $P = 0.535$). However, photoconversion to *trans*-BAI significantly increased the oscillatory frequency (0.63 ± 0.10 to 0.81 ± 0.09 Hz, $P = 0.038$) due to a significant reduction in Down-state duration (from 1.99 ± 0.43 s during *cis*-BAI to 1.47 ± 0.29 s after *trans*-BAI, $P = 0.038$). Data are presented as means \pm SD; P-values: * ≤ 0.05 ; ** ≤ 0.01 ; ns = not significant. Statistical analysis was performed using the two-sided Mann–Whitney U test.

trans-BAI, $P = 0.0286$). 1 and 2 μ M *cis*-BAI applications resulted in a lower increase in the oscillatory frequency compared with *trans*-BAI (from 0.47 ± 0.03 Hz during control to 0.66 ± 0.04 Hz with 2 μ M *cis*-BAI, $P = 0.0079$). Significant differences were observed in the oscillatory frequency values between the two isoforms at these concentrations (1 μ M $P = 0.0317$; 2 μ M $P = 0.0079$). However, at 3 μ M of the preilluminated BAI solution (*cis*-enriched form), the content of *trans*-isomer may have been higher than at lower concentrations and could have prevented significant differences in slices.

In summary, both *trans*- and *cis*-BAI were able to modulate SO toward a faster wave activity in a dose-dependent manner at 1 and 2 μ M. However, *trans*-BAI showed significantly stronger agonism at these concentrations. The identification of this suitable concentration window allowed us to optimize the direct application of light for controlling M_1 mAChR activity and modulating cortical SO in cortical slices in vitro.

BAI increases the frequency of slow waves in vitro

Once the optimal range of drug concentration was identified, we proceeded to control SO activity with photoswitchable BAI in cortical slices (Fig. 2c). We recorded baseline SO as a control condition and then applied 1 μ M of *cis*-BAI under dark conditions to avoid conversion to *trans*-BAI (15). Compared with the control condition, the frequency of oscillation under 1 μ M *cis*-BAI showed no

significant changes (from 0.53 ± 0.11 Hz during control to 0.55 ± 0.16 Hz; $n = 9$; $P = 0.920$), as expected. Subsequent illumination of the slices with white light produced the photoconversion of BAI (Fig. 1a) into the *trans*-isomer, resulting in a significant increase in the oscillatory frequency (from 0.53 ± 0.11 Hz during control to 0.83 ± 0.06 Hz with 1 μ M of *trans*-BAI, $P = 0.003$) (Fig. 2d). This increase was associated with a decrease in the duration of the Down-state periods (from 2.19 ± 0.60 s during control to 1.64 ± 0.93 s with 1 μ M *trans*-BAI, $P = 0.034$). No significant changes were observed in the firing rate (FR) or duration of the Up state (Table S1a) during photoconversion of BAI. This result provides a mechanistic insight into the network dynamics and its modulation that points toward network excitability during Down states (20, 23).

BAI increases the frequency of slow waves in vivo

To determine whether the impact of the photoswitchable M_1 agonist BAI on slow oscillatory activity was not only limited to cortical slices but also evident in the brain in situ, we conducted recordings of activity from the primary visual cortex (V1) from anesthetized mice. While in cortical slices the drug application was directly over the cortical parenchyma, in vivo the drug application was done over the pia mater. Due to this different route of drug administration, we increased the concentration of the locally applied drug to 5 μ M (16) (Fig. 3a). This is in agreement with previous findings where the required concentration of photoswitchable M_2 agonist PAI was

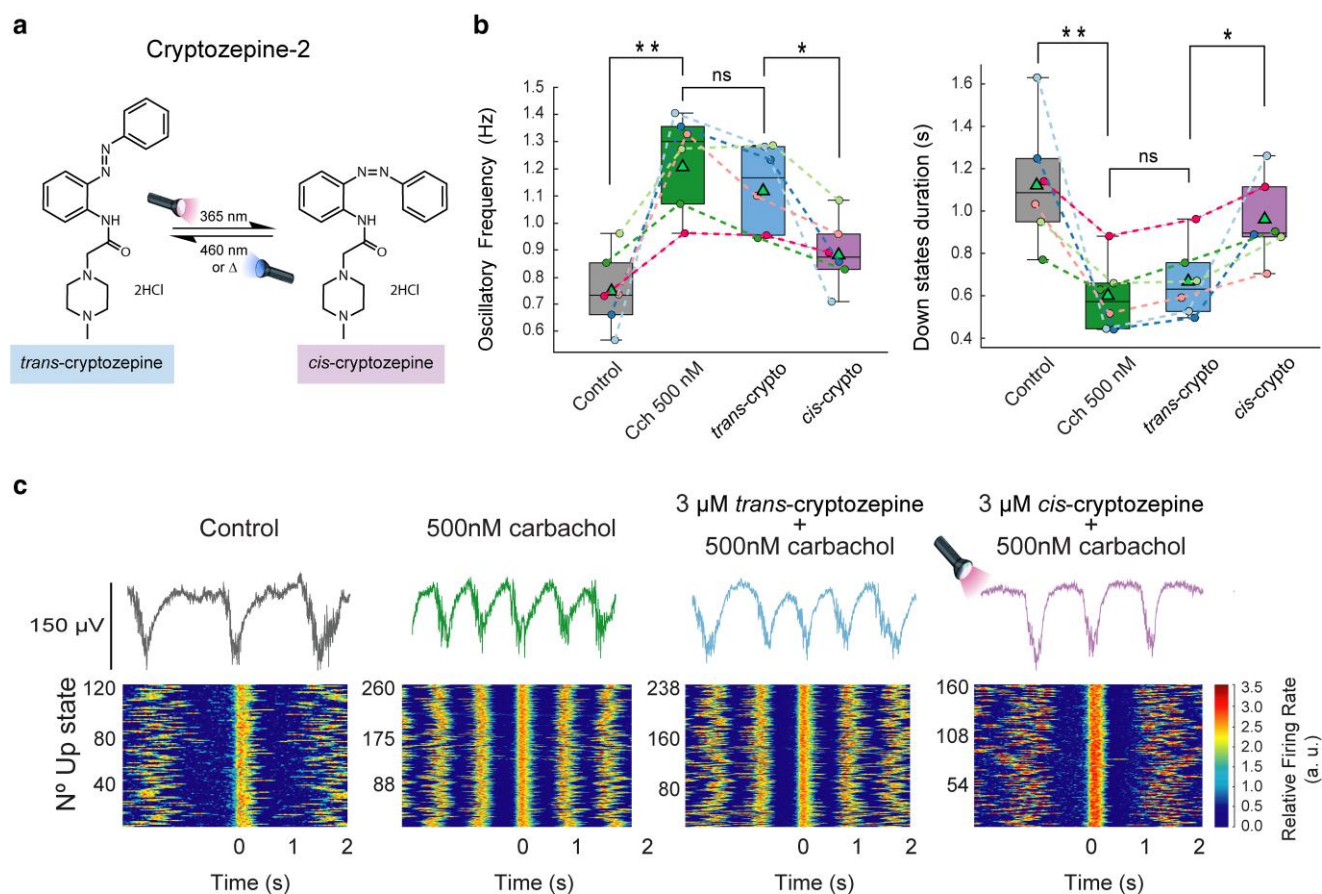


Fig. 4. Photocontrol of SO with cryptozepine and direct illumination with UV light in vitro. **a**) Chemical structures of the *cis*- and *trans*-isomers of cryptozepine, along with the wavelengths required for their photoswitching. **b**) Boxplots with individual data points representing the median values (dark line) and mean values (green triangles) of oscillatory frequency (Hz) and Down-state duration (s) under the different conditions. Application of 500 nM CCh significantly increased oscillatory frequency (from 0.75 ± 0.13 to 1.23 ± 0.16 Hz, $n = 6$ brain slices, $P = 0.002$). The subsequent addition of 3 μM *trans*-cryptozepine caused no significant change in oscillatory frequency (from 1.23 ± 0.16 to 1.13 ± 0.14 Hz, $P = 0.240$). However, UV light illumination, which triggered the conversion to *cis*-cryptozepine, resulted in a significant decrease in oscillatory frequency (from 1.13 ± 0.14 to 0.96 ± 0.18 Hz, $P = 0.040$), characterized by an elongation of the Down-state duration (from 0.66 ± 0.16 s with CCh and *trans*-cryptozepine to 0.93 ± 0.18 s with CCh and *cis*-cryptozepine, $P = 0.040$). **c**) Representative LFP traces (top) and raster plot of relative FR (bottom) recorded from cortical slices during the different experimental conditions: control, application of M_{1-5} muscarinic agonist carbachol (500 nM CCh), addition of 500 nM CCh + 3 μM *trans*-cryptozepine (inactive isomer of the M_1 mAChR antagonist), and after photoconversion with UV light to 500 nM CCh + 3 μM *cis*-cryptozepine (active isomer). Data are presented as means \pm SD; P-values: * ≤ 0.05 ; ** ≤ 0.01 ; ns = not significant. Statistical analysis was performed using the two-sided Mann–Whitney U test.

5-fold higher in vivo than in vitro (1 μM vs. 200 nM) (16). Compared with control activity, application of *cis*-BAI did not result in significant changes in the frequency of SO (from 0.63 ± 0.10 Hz during control to 0.67 ± 0.12 Hz under 5 μM *cis*-BAI, $n = 7$, $P = 0.535$). However, following direct white-light illumination of the cortex, *cis*-BAI switched to its *trans* active isomer, resulting in a significant increase in the oscillatory frequency (from 0.63 ± 0.10 Hz during control to 0.81 ± 0.09 Hz, $P = 0.038$; Fig. 3b) mainly due to a significant decrease in the Down-state duration (from 1.99 ± 0.43 s during *cis*-BAI to 1.47 ± 0.29 s during *trans*-BAI, $P = 0.038$). No significant changes were observed in the FR or duration of the Up state (Table S1b) during photoconversion of BAI. These results are aligned with what was empirically observed in the cortex in vitro.

Cryptozepine blocks the muscarinic effects on SO

To further understand the role of the M_1 mAChR on cortical dynamics, we investigated the effect of the recently reported photo-switchable M_1 mAChR antagonist cryptozepine (18) on SO. We initially tested the photoswitchable *trans*-cryptozepine (inactive) and *cis*-cryptozepine (active) isomer antagonists of M_1 mAChRs

at 1, 10, and 100 μM concentrations in the presence of the muscarinic agonist carbachol at 1 μM (Fig. S3; $n = 2$ for each concentration). Based on these preliminary experiments, a concentration of 3 μM cryptozepine was chosen to effectively block the effects of 500 nM carbachol by light (Fig. 4; $n = 6$).

The SO activity (control condition) was initially recorded as baseline. Following the application of 500 nM carbachol, the oscillatory frequency significantly increased (from 0.75 ± 0.13 Hz in control condition to 1.23 ± 0.16 Hz, $n = 6$, $P = 0.002$; Fig. 4b). Next, 3 μM *trans*-cryptozepine was added, without a significant reduction in oscillatory frequency (from 1.23 ± 0.16 to 1.13 ± 0.14 Hz, $P = 0.240$), as expected. Illumination of the brain slices with 365-nm light triggered the *trans*- to *cis*-cryptozepine photoconversion, causing a significant decrease in the frequency of oscillation (from 1.13 ± 0.14 to 0.96 ± 0.18 Hz, $P = 0.040$) and therefore blocking the carbachol effects. This change in activity was characterized by an elongation of the Down-state period (from 0.66 ± 0.16 s during 500 nM carbachol and 3 μM *trans*-cryptozepine to 0.93 ± 0.18 with 500 nM carbachol and 3 μM *cis*-cryptozepine, $P = 0.04$). No significant changes were observed in the FR or duration of the Up state (Table S2) during photoconversion of cryptozepine.

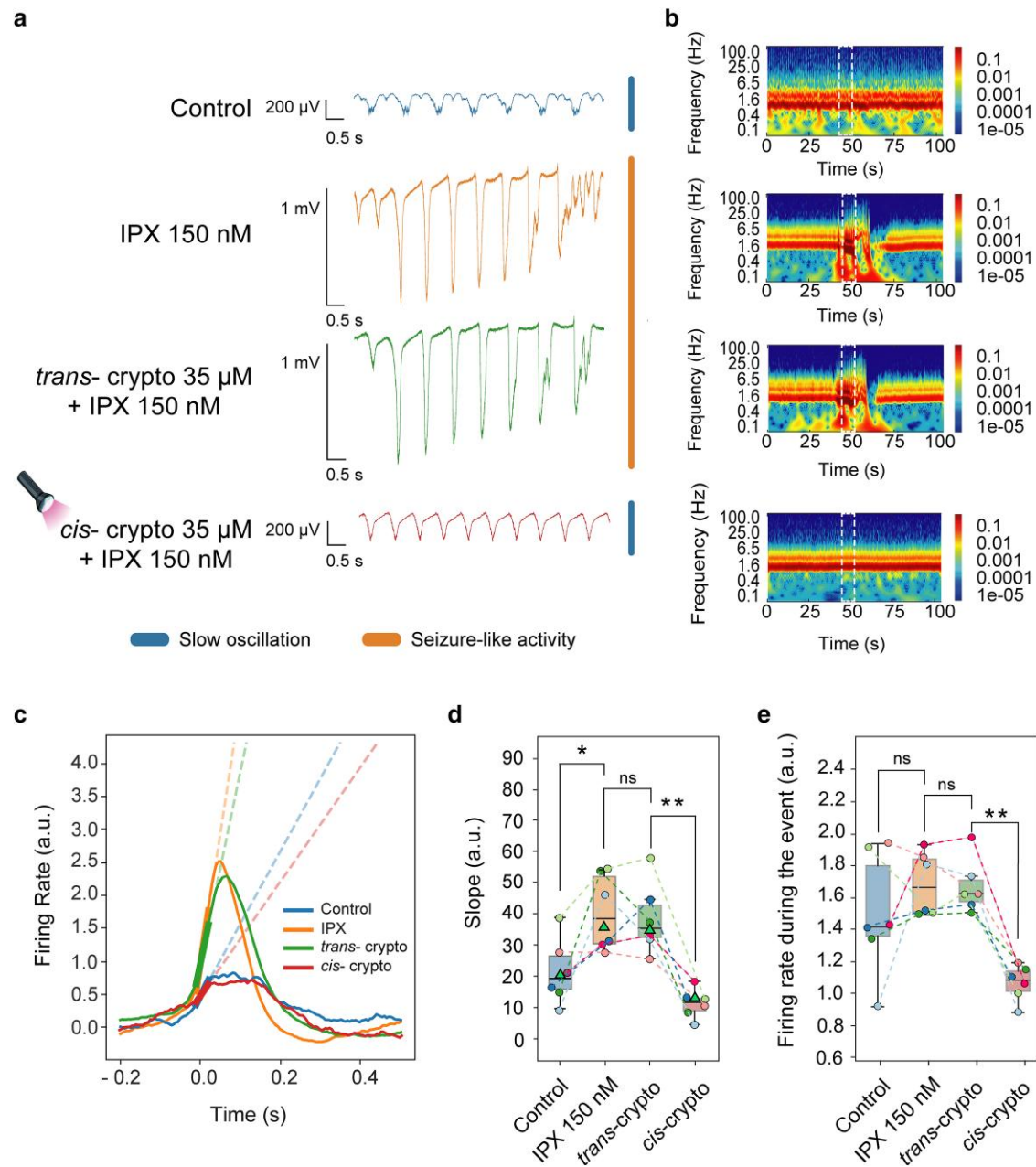


Fig. 5. Blockade of seizure-like activity with photoswitchable cryptozepine in vitro. a) Representative LFP traces recorded from cortical slices under different conditions: control (spontaneous SO), bath application of 150 nM IPX, which induces seizure-like activity, 150 nM IPX + 35 μ M *trans*-cryptozepine (inactive isomer, without blockade of seizure-like activity), and after photoconversion with UV light to 150 nM IPX + 35 μ M *cis*-cryptozepine (active isomer), which blocks seizure-like discharges and restores the SO. b) Representative spectrograms showing the frequency power spectra for each condition, illustrating the transition from SO to seizure-like activity under IPX and the return to SO following photoconversion of cryptozepine. c) FR during the transition from Down state to spiking states (either Up state or epileptic discharges, a.u.) across conditions. The slope of the transition is calculated by fitting the FR during the period from -0.01 to 0.025 s relative to the transition onset (dashed line), indicating how quickly and strongly the network is recruiting the subsequent spiking events. d) Boxplots with individual data points representing the median values (black line) and mean values (green triangles) of the transition slope (a.u.) during the transition from Down state to the next spiking event. Upon application of 150 nM IPX, the slope significantly increased (from 21.33 ± 7.84 a.u. during control to 35.03 ± 9.31 a.u., $n = 6$ brain slices, $P = 0.026$). Following UV light-induced photoconversion of cryptozepine from *trans* to *cis* (35 μ M + 150 nM IPX), the slope decreased significantly (from 34.03 ± 8.73 a.u. to 13.41 ± 3.53 a.u., $P = 0.0022$). e) Boxplots with individual data points representing the median values (black line) and mean values (green triangles) of the FR (a.u.) during the previous conditions. The FR decreased significantly after photoconversion of cryptozepine (from 1.74 ± 0.27 a.u. with *trans*-cryptozepine + 150 nM IPX to 0.91 ± 0.15 a.u. with *cis*-cryptozepine + 150 nM IPX, $P = 0.0022$), corresponding to the blockade of seizure-like activity and recovery of the SO regime. Data are presented as means \pm SD; P-values: * ≤ 0.05 ; ** ≤ 0.01 ; ns = not significant. Statistical analysis was performed using the two-sided Mann-Whitney U test.

Cryptozepine blocks muscarinic-induced seizure-like activity in vitro

As previously described (16), the nonsubtype-selective mAChR superagonist iperoxo (IPX) induced seizure-like activity in cortical slices in vitro (Fig. S4a). We found that high concentrations (30 μ M

trans-BAI) also induced cyclic periods of seizure-like activity (Fig. S4b), which was not observed during application of the M_2 agonist PAI. Only after bath application of M_1 mAChR antagonist pirenzepine (PNZ) was it possible to reverse the epileptogenic discharges (Fig. S4c) evoked by IPX. This strongly supports the notion

that M_1 mAChRs play a pivotal role in mediating these hypersynchronous events within the cortical network, as previously proposed (24).

To study and quantify the transition from SO to highly synchronized discharges during seizure-like activity, we measured the slope of multiunit activity (MUA) during the transition from Down state and the FR to the next discharge event (which could be either Up states during SO or epileptogenic discharges during seizure-like activity). These measures are directly related to how fast networks are recruited and how strong they are firing in these epileptiform periods (25). Both slope and FR were found to increase during epileptogenic activity in vitro (Fig. S4e and f).

Following this evidence, we tested the light-mediated effect of *trans*-cryptozepine (inactive isoform) and *cis*-cryptozepine (active isoform) at 35 μ M in the presence of 150 nM IPX (Fig. 5a). We initially recorded the SO as a control condition and then applied 150 nM IPX evoking high-amplitude seizure-like activity. First, the slope of MUA was significantly increased in the transition from Down state to the next event with IPX (from 21.33 ± 7.84 a.u. during the control condition to 35.03 ± 9.31 a.u. with IPX 150 nM, $P = 0.026$; Fig. 5c). Subsequent application of *trans*-cryptozepine had no evident effect on the seizure-like activity. *Trans*- to *cis*-photoconversion of cryptozepine from direct 365-nm illumination of the brain slices changed the pattern of discharge of the seizures to SO. Although physiological oscillations were restored, oscillatory frequency after illumination remained faster compared with the control condition (Fig. 5b), probably due to activation of M_2 mAChRs using PAI, as previously reported (16). The slope was significantly decreased (from 34.03 ± 8.73 a.u. with 35 μ M *trans*-cryptozepine + 150 nM IPX to 13.41 ± 3.53 a.u. with 35 μ M *cis*-cryptozepine + 150 nM IPX, $n = 6$, $P = 0.0022$, Fig. 5d) as well as the FR during the event (from 1.74 ± 0.27 a.u. with 35 μ M *trans*-cryptozepine + 150 nM IPX to 0.91 ± 0.15 a.u. 35 μ M *cis*-cryptozepine + 150 nM IPX, $P = 0.0022$, Fig. 5e).

In summary, we demonstrate that the M_1 mAChRs play an important role in cholinergic-induced seizure-like activity and that photoswitchable antagonist cryptozepine can specifically modulate muscarinic-induced seizure-like activity through illumination.

Discussion

In this study, we have demonstrated that using light to activate the photoswitchable M_1 mAChR agonist BAI allows precise control of cortical network activity, including a significant increase in the frequency of SO in the cortex. These effects were observed not only in isolated cortical preparations in vitro but also in anesthetized animals. Furthermore, we achieved light-mediated blockade of M_1 mAChRs using the innovative photoswitchable antagonist, cryptozepine, effectively mitigating the effects of muscarinic agonist carbachol on SO and reversing seizure-like activity induced by the superagonist IPX.

In summary, our findings offer new insights into the role of M_1 mAChRs in shaping cortical dynamics. Additionally, they underscore the capacity of photoswitchable M_1 ligands to accurately control both normal and pathological cortical activity using light.

Cholinergic activation is a driving force behind waking from sleep, contributing to the transition from SO, synchronized (sleep) activity patterns to the desynchronized patterns that are associated with wakefulness and conscious processing (26–28). Cholinergic drugs have been used to reverse the effects of anesthesia, an action attributed to nicotinic AChRs and M_1 and M_4 mAChRs (29). Interestingly, an increase in SO frequency like that induced by light activation of BAI, along with the shortening of Down states, was also found in the transition from deep anesthesia to light

anesthesia (30–32). The increase in oscillatory frequency and the shorter duration of Down states can be explained by heightened excitability caused by the blockade of Kv7 potassium channels, which is a result of the action of M_1 agonists (33, 34).

In a prior study (16), we demonstrated that PAI, an M_2 -selective derivative of IPX, did not induce epileptogenic activity despite enhancing excitability. In contrast, our current findings reveal that high concentrations of the M_1 -selective ligand BAI can replicate the epileptiform discharges observed with nonsubtype-selective IPX (Fig. S4a). This distinction in network excitability mediated by M_1 mAChRs (resulting in seizure-like activity) and M_2 mAChRs (leading to an increase in SO frequency) could arise from the differences in intracellular pathways associated with these two mAChR subtypes (8). Moreover, M_1 mAChRs are predominantly expressed postsynaptically on pyramidal cells, while M_2 mAChRs are primarily found presynaptically and work as heteroreceptors inhibiting GABA release (35, 36). Besides these differences, selective activation of M_1 and M_2 mAChRs synergistically enhanced excitability of the network increasing oscillatory frequency.

Selective photoswitchable ligands have proven to be a useful method to disclose muscarinic subtype selective mechanisms of cortical dynamics without requiring genetic modifications. While BAI exhibits potential in modulating SO, it is essential to acknowledge existing limitations that need to be addressed for its full realization. A primary limitation lies in the efficacy of BAI as a photoswitchable ligand, which is confined to a narrow concentration range (1–2 μ M). BAI also shows a mild effect on oscillatory frequency compared with other nonphotoswitchable muscarinic agonists like carbachol. While these limitations may pose challenges for clinical applications, it is worth noting that many M_1 positive allosteric modulators lacking a strong affinity for M_1 mAChRs have demonstrated cognitive enhancement benefits without the typical epileptic side effects associated with more potent M_1 agonists (37).

In addition, innovative illumination devices could be implanted in specific regions of the brain cortex with minimal invasiveness to photoconvert *cis*- to *trans*-BAI. In a hypothetical clinical context, BAI would be administered systematically after 365-nm irradiation to obtain *cis*-BAI and then selectively activated by light in the brain. This approach could be relevant in the treatment of pathologies like Alzheimer's disease where M_1 mAChRs have a pivotal role (7, 38–40) in treating conditions such as stroke, in which perilesional cortical regions are dominated by slow-wave states in awake subjects (13, 41, 42), or in disorders of consciousness (14). Of course, many aspects need to be further evaluated for the clinical translation of BAI, such as concentration ranges in humans optimal for photoswitching, photosensitivity, toxicity levels, and blood–brain barrier permeability.

Cryptozepine allowed us to effectively reverse the effect of the muscarinic agonist carbachol in SO by photoswitching its M_1 antagonism. Photoactivation of cryptozepine and blockade of M_1 mAChRs resulted in a significant elongation of Down states and therefore a decrease in the oscillatory frequency. No significant changes were observed in the FR or duration of Up states (Table S2) contrary to the elongation of Up states reported in previous studies using the M_1 antagonist PNZ (43). It is important to emphasize that further in vivo experiments without the use of cholinergic agonists are necessary to fully understand the effects of cryptozepine photoconversion on the endogenous cholinergic system.

We have demonstrated the effectiveness of cryptozepine in blocking the epileptogenic effects of IPX. To our knowledge, this is the first application of photopharmacology reversing epileptogenic events in the brain, providing a breakthrough for using

cryptozepine as a photopharmacological technology for studying and controlling muscarinic-induced seizures (44). Moreover, the results further highlight the relevance of M_1 mAChRs in hypersynchronous events such as seizures (45). By using light-mediated activation of the antagonist, it should be possible to modulate neuronal excitability during epileptic events. Due to local activation of the antagonist, the negative impact on hippocampus-dependent learning typically observed with the use of anticonvulsants could be avoided (46, 47). A notable limitation of cryptozepine's photoconversion to its active isoform is the requirement for UV light, which not only limits tissue penetration but also poses the risk of causing potential damage to neuronal DNA (48). There is therefore a need to design new photoswitchable drugs that are susceptible to activation/deactivation with red or infrared light to improve tissue penetration and minimize damage (49, 50).

In summary, our findings indicate that M_1 mAChRs can effectively regulate both physiological SO and pathological epileptic discharges in the cortex. By utilizing photoswitchable M_1 mAChR ligands, we were able to achieve selective modulation of these neural patterns through light stimulation, without the need for gene manipulation. This approach offers a powerful tool for investigating cortical dynamics and exploring potential therapies for patients who are unresponsive to conventional treatments.

Materials and methods

Cell culture and transient transfection

Human embryonic kidney tsA201 (HEK tsA201, American Type Culture Collection [ATCC]) cells were maintained in Dulbecco's modified Eagle's medium/nutrient mixture F-12 Ham (DMEM/F12 1:1, Life Technologies, Carlsbad, CA, USA) supplemented with 10% fetal bovine serum (FBS, Life Technologies) and penicillin and streptomycin (1%, Sigma-Aldrich, St. Louis, MI, USA) in a controlled environment (37 °C, 98% humidity, and 5% CO₂).

The cells were transiently transfected with the human M_1 mAChR (Addgene, Watertown, MA, USA) or co-transfected with the human M_2 mAChR (Addgene) and chimeric G_i/G_q protein (G_{qTOP}) (ratio 1:1) using X-tremeGENE 9 DNA Transfection Reagent (Roche Applied Science, Penzberg, Germany) following the manufacturer's instructions. M_1 mAChR preferentially activates G_q proteins and leads to the activation of the phospholipase $C\beta$ (PLC β) pathway, resulting in the production of inositol 1,4,5-trisphosphate (IP₃) and the subsequent release of intracellular calcium from the endoplasmic reticulum. In contrast, the M_2 mAChR prevalently activates G_i proteins; therefore, we co-transfected the cells with a chimeric $G_{q/i}$ -protein (G_{qTOP}), which couples M_2 mAChR activation with the PLC β pathway (19). One day later, cells were harvested with Accutase (Sigma-Aldrich) and seeded onto 16-mm glass coverslips (Fisher Scientific, Hampton, NH, USA) coated with poly-L-lysine (Sigma-Aldrich) to allow cell adhesion. Finally, the seeded cells were used for the experiments after 24 h.

In vitro single-cell calcium imaging

The calcium imaging assay was performed in the HEK tsA201 cell line using a calcium indicator (i.e. OGB-1 AM) to determine changes in intracellular calcium concentrations upon receptor activation.

The bath solution used for single-cell intracellular calcium recordings contained 140 mM NaCl, 5.4 mM KCl, 1 mM MgCl₂, 10 mM HEPES, 10 mM glucose, and 2 mM CaCl₂ (pH 7.4). The calcium indicator used to test BAI was OGB-1 AM (Life Technologies). Before each experiment, cells were mounted on the recording chamber (Open Diamond Bath Imaging Chamber for Round Coverslips from

Warner Instruments, Hamden, CT, USA) and loaded with OGB-1AM for 30 min at 37 °C with 5% CO₂ at a final concentration of 10 μ M in Ca²⁺-free bath solution. Cells were rinsed with fresh solution, and the recording chamber was filled with 1 mL of recording solution and placed on an IX71 inverted microscope (Olympus, Tokyo, Japan) with a XLUMPLFLN 20XW 20 \times water immersion objective (Olympus). OGB-1 AM was excited for 50 ms at 488 nm using a Polychrome V light source (Till Photonics, Victor, NY, USA) equipped with a Xenon Short Arc lamp (Ushio, Steinhöring, Germany) and a 505-nm dichroic beam splitter (Chroma Technology, Olching, Germany). Emission at 510 nm was filtered using a D535/40-nm emission filter (Chroma Technology) and finally collected with a C9100-13 EM-CCD camera (Hamamatsu, Shizuoka, Japan). Images were acquired at room temperature with an imaging interval of 4 s with SmartLux software (HEKA), and the imaging analysis was executed with FIJI (ImageJ). The change in fluorescence intensity over time is represented as F/F_0 , where F is the intensity of fluorescence emission recorded as the experiment runs and F_0 is a measure of the baseline fluorescence at the start of the experiment.

The agonist used to stimulate M_1 and M_2 mAChRs in HEK tsA201 cells was ACh (Sigma-Aldrich). Application of vehicle (0.1% dimethyl sulfoxide [DMSO]), BAI, and ACh was carried out by manually pipetting a small volume during imaging acquisition into the accessory pool of the recording chamber for the final dilution of ~1:1,000.

Photostimulation under 1PE during recordings was done by illumination of the entire focused field using the Polychrome V connected to a PC. Shutter and wavelength were controlled using Patchmaster software (HEKA). For all the HEK cell experiments, the light intervals lasted a total of 5 min, with flashes of blue (460 nm, 3.5-s duration) and UV (365 nm, 3.5-s duration) light. The light power measured with a Newport 1916-C light meter placed after the objective was 16 W·m⁻² for 488 nm, 5 W·m⁻² for 365 nm, and 16 W·m⁻² for 460 nm.

Preparation of cortical slices in vitro

Isolated cortical slices of ferret fully reproduce SO compared with other species (51). For this reason, cortical electrophysiology experiments were carried out in 3–7-month-old ferrets, either sex. All experiments were performed in accordance with protocols approved by the Animal Ethics Committee of the University of Barcelona, which comply with the European Union guidelines on the protection of vertebrates used for experimentation (Directive 2010/63/EU of the European Parliament and the Council of 2010 September 22).

Cortical slices were prepared as previously described (26). Briefly, ferrets were anesthetized with sodium pentobarbital (40 mg/kg) and decapitated. The entire forebrain was rapidly removed to an oxygenated cold (4–10 °C) bathing medium and cut into 400- μ m-thick coronal slices (Microm HM 650 V, Thermo Fisher, Waltham, MA, USA) from the occipital cortex containing primary and secondary visual cortical areas (areas 17, 18, and 19). To increase tissue viability, a modification of the sucrose substitution technique developed by Aghajanian and Rasmussen (52) was used during the preparation. Sucrose-substituted solution used during slicing contains (in mM): sucrose, 213; KCl, 2.5; NaH₂PO₄, 1; NaHCO₃, 26; CaCl₂, 1; MgSO₄, 3; and glucose, 10.

For the first 30 min in the interphase chamber, cortical slices were superfused with a 1:1 mixture of artificial cerebrospinal fluid (ACSF) and a sucrose-substituted solution. After this initial period, the normal bathing medium was introduced into the recording chamber, and the slices were continuously superfused for an additional 1–2 h. The composition of the ACSF was (in mM): NaCl, 126; KCl, 2.5; MgSO₄, 2; Na₂HPO₄, 1; CaCl₂, 2; NaHCO₃, 26; and glucose,

10. It was aerated with a gas mixture of 95% O₂ and 5% CO₂ to maintain a final pH of 7.4. For the rest of the experiment, a modified ACSF was used, with the same ionic composition except for adjusted concentrations of KCl (4 mM), MgSO₄ (1 mM), and CaCl₂ (1 mM) (11). The bath temperature was maintained at 34–36 °C.

Recording of cortical activity and data analysis

Extracellular local field potential (LFP) from cortical slices was recorded after recovery using tungsten electrodes (FHC, CA, USA). Signals were amplified 100-fold using a PGA16 multichannel system amplifier (MCS, Reutlingen, Germany), digitized with a Power 1401 CED (CED, Cambridge, UK) at a 5-kHz sampling rate, and acquired using Spike2 software (CED, Cambridge, UK). We analyzed spontaneous population-level spiking events corresponding to cortical Up states, followed by silent Down states. To capture this activity, raw LFP signals (Fig. 2a) were band-pass filtered between 200 and 1,500 Hz, isolating MUA (53), which reflects the firing patterns of the local cortical network. To mitigate large signal fluctuations, the MUA was logarithmically transformed (logMUA). Analysis of the MUA signal revealed a bimodal distribution, with two prominent peaks corresponding to the network activity during the Up and Down states. To differentiate between these states, a threshold value was set between the two peaks. This allowed us to classify samples as belonging to either the Up or Down states based on their relative positions to this threshold (54).

This method allowed for the precise identification of up-to-Down and Down-to-up state transitions. From these transition times, we calculated the duration of both Up and Down states, which were represented at the population level using boxplots. The FR during each Up state was determined by averaging the logMUA over the Up state duration. The slope of the Down state to the next active/spiking event (epileptogenic discharge or Up state) was computed by fitting a line over the FR data samples surrounding the transition point (−10 to 25 ms).

Recording in mouse neocortex in vivo

Cortical electrophysiology experiments in vivo were carried out in 2–3-month-old C57BL6/JR mice, following the European Union Directive 2010/63/EU, and approved by the local ethics committee (Ethics Committee of Animal Experimentation of the University of Barcelona, CEEA-UB). Mice were kept under standard conditions (room temperature, 12:12-h light–dark cycle, lights on at 8:00 AM). Anesthesia was induced by intraperitoneal injection of ketamine (30 mg/kg) and medetomidine (100 mg/kg). The mice were fixed in a stereotaxic frame, and the body temperature was maintained at 37 °C throughout the experiment. A craniotomy was performed in each mouse in the primary visual cortex, V1; coordinates: AP −2.5 mm, L 1.5 mm). Later, a well was made using dental cement and the cis-BAI was delivered in the craniotomy. LFP was recorded from deep layers using a 16-channel multielectrode array; the probe consisted of one shank with 16 linearly spaced sites at 100 μm (ATLAS Neuroengineering, Leuven, Belgium) enabling recording throughout the cortical column. Same amplification, digitalization, and filtering systems were used as in in vitro recordings.

Drug application

BAI is a dualsteric agonist composed of IPX (the orthosteric moiety), azobenzene (photoswitchable spacer chain), and the benzyl quinolone carboxylic acid (allosteric moiety, M₁ mAChR positive allosteric modulator, Fig. 1a). BAI was developed by Agnetta et al. (17). Stock solution (10 mM) was prepared by dissolving the compound in 98% DMSO (Sigma).

To study the effect of BAI on cortical dynamics in vitro, first we applied the BAI cis isomer, which has a lower affinity for M₁ mAChRs (inactive molecule). Then, we applied UV light (Vilber Lourmat Dual Wave Length UV Lamps, 365 nm 6 W) for 5 min to the BAI stock dilution (100 μM) with ACSF, which was then further diluted to 1 μM BAI and added to the interphase chamber bath in the dark. Finally, we applied white light directly to the brain slice to obtain the trans-isomer (active molecule, Fig. 2c). We waited 1,000 s in each condition (control, cis-BAI, and trans-BAI) to observe the effects of the BAI isomers. In the in vivo experiments, cis-BAI was delivered to the dental cement well following the same experimental sequence as in vitro. The BAI concentration used in vivo was five times higher (5 μM) than that used in vitro, as previously described for this type of drug delivery (16).

Cryptozepine is a modified PNZ (M₁ mAChR antagonist) with an azobenzene chain, which allows photoconversion from trans-cryptozepine (less active isomer) to cis-cryptozepine (isomer with a stronger affinity for M₁ mAChRs, Fig. 4a) when exposed to 365-nm light (UV light), and it back-isomerizes to trans when exposed to 460-nm light or white light.

To reproduce physiological levels of cholinergic activation on brain slices, we used the nonselective muscarinic agonist carbachol due to a limited number of cholinergic neurons in the neocortex that physiologically release ACh. Carbachol was applied to the recording chamber at a concentration of 0.5 μM. Next, we added the lower-affinity isomer 3 μM trans-cryptozepine and exposed the chamber to 10 min of UV light to obtain the more active isomer cis-cryptozepine. To reproduce epileptiform cortical patterns, we used the nonselective muscarinic superagonist IPX, allowing overactivation of muscarinic receptors. IPX was applied to the recording chamber at a concentration of 150 nM. Next, we added the lower-affinity isomer 35 μM trans-cryptozepine and exposed the chamber to 10 min of UV light to obtain the more active isomer cis-cryptozepine.

We waited for 1,000 s in each condition (control, trans-, and cis-) to observe the effects of the cryptozepine isomers. The UV-light lamp (Vilber Lourmat, 365 nm 6W) was positioned with a 45° tilt and at a 4-cm distance from the slices to achieve harmless long-lasting UV exposure providing enough photoconversion of cryptozepine from trans- to cis-isomers to reverse the effects of carbachol or IPX.

Statistical analysis

Numerical data from calcium imaging experiments were imported to GraphPad Prism version 6.00 for Windows (GraphPad Software, La Jolla, CA, USA). Statistical analysis was performed using one-way ANOVA followed by Tukey's post hoc test (Fig. 1d), the paired-sample Wilcoxon signed-rank test (Fig. 1e), and an unpaired t test with Welch's correction (Fig. S1). The data were normalized over the maximum response obtained with ACh at 1 μM and analyzed and presented as mean ± SEM. P-values were as follows: * ≤ 0.05; ** ≤ 0.01; *** ≤ 0.001; and **** ≤ 0.0001.

Statistical analysis for both in vitro and in vivo electrophysiology data was performed using the Mann–Whitney U test. Data are presented as mean ± SEM throughout the text; boxplots indicate median values, green triangles indicate mean values, and individual data points are shown to illustrate the distribution of the samples. P-values were as follows: * ≤ 0.05 and ** ≤ 0.01.

Acknowledgments

The authors thank Tony Donegan for his help with language editing.

Supplementary Material

Supplementary material is available at PNAS Nexus online.

Funding

This work has received funding from the European Union's Horizon 2020 Framework Programme for Research and Innovation under the Specific Grant Agreement No. 945539 (Human Brain Project SGA3) to M.V.S.-V. and P.G., EBRAINS-PREP 101079717 to M.V.S.-V., and by the Generalitat de Catalunya -AGAUR- (IU16-011508) to P.G. and M.V.S.-V. J.M.S.-S. was supported by a predoctoral fellowship Formación de Personal Investigador (FPI) (reference PRE2018-086203). R.S. was supported by a predoctoral fellowship FPI (reference BES-2017-082496). P.G. research was funded by DEEPER (ICT-36-2020-101016787); European Research ERA-Net SynBio Programme (Modulightor project); Generalitat de Catalunya (CERCA Programme; 2017-SGR-1442 project); and Ministry of Economy and Competitiveness (MINECO)/FEDER (Grant CTQ2016-80066-R, the Fundaluce Foundation). M.V.S.-V. research was funded by Spanish grants PID2023-152918OB-I00 financed by MICIU / AEI / 10.13039/501100011033 and AGAUR 2021-SGR-01165.

Data Availability

All drugs used in this work have been synthesized and characterized as described in the corresponding references and can be obtained from the authors. Data analysis tools are available at <https://doi.org/10.1016/j.crmeth.2023.100681>, code at <https://github.com/NeuralEnsemble/cobrawap>, and cortical data in EBRAINS at <https://doi.org/10.25493/PYDG-9KZ> and <https://search.kg.ebrains.eu/instances/03fc9ac7-ae06-4bd8-946f-1da3749aca64>.

References

- Luria AR, Haigh B. *Higher cortical functions in man*. 2nd ed. Springer, 1980.
- Bamberg E, Gärtner W, Trauner D. 2018. Introduction: optogenetics and photopharmacology. *Chem Rev*. 118:10627–10628.
- McCormick DA, Nestvogel DB, He BJ. 2020. Neuromodulation of brain state and behavior. *Annu Rev Neurosci*. 43:391–415.
- Lee S-H, Dan Y. 2012. Neuromodulation of brain states. *Neuron*. 76:209–222.
- Carrera-Cañas C, Garzón M, de Andrés I. 2019. The transition between slow-wave sleep and REM sleep constitutes an independent sleep stage organized by cholinergic mechanisms in the rostradorsal pontine tegmentum. *Front Neurosci*. 13:748.
- Hasselmo ME, Giocomo LM. 2006. Cholinergic modulation of cortical function. *J Mol Neurosci*. 30:133–135.
- Caccamo A, et al. 2006. M1 receptors play a central role in modulating AD-like pathology in transgenic mice. *Neuron*. 49:671–682.
- Brown DA. 2010. Muscarinic acetylcholine receptors (mAChRs) in the nervous system: some functions and mechanisms. *J Mol Neurosci*. 41:340–346.
- Kruse AC, et al. 2014. Muscarinic acetylcholine receptors: novel opportunities for drug development. *Nat Rev Drug Discov*. 13:549–560.
- Eglen RM. Muscarinic receptor subtype pharmacology and physiology. *Progress in medicinal chemistry*. Elsevier, 2005. p. 105–136.
- Sanchez-Vives MV, McCormick DA. 2000. Cellular and network mechanisms of rhythmic recurrent activity in neocortex. *Nat Neurosci*. 3:1027–1034.
- Sanchez-Vives MV, Massimini M, Mattia M. 2017. Shaping the default activity pattern of the cortical network. *Neuron*. 94:993–1001.
- Sarasso S, et al. 2020. Local sleep-like cortical reactivity in the awake brain after focal injury. *Brain*. 143:3672–3684.
- Rosanova M, et al. 2018. Sleep-like cortical OFF-periods disrupt causality and complexity in the brain of unresponsive wakefulness syndrome patients. *Nat Commun*. 9:4427.
- Rieffolo F, et al. 2019. Optical control of cardiac function with a photoswitchable muscarinic agonist. *J Am Chem Soc*. 141:7628–7636.
- Barbero-Castillo A, et al. 2021. Control of brain state transitions with a photoswitchable muscarinic agonist. *Adv Sci*. 8:e2005027.
- Agnetta L, et al. 2017. A photoswitchable dualsteric ligand controlling receptor efficacy. *Angew Chem Int Ed*. 56:7282–7287.
- Rieffolo F, et al. 2021. Rational design of photochromic analogues of tricyclic drugs. *J Med Chem*. 64:9259–9270.
- Gomez J, et al. 1996. Coupling of metabotropic glutamate receptors 2 and 4 to G alpha 15, G alpha 16, and chimeric G alpha q/i proteins: characterization of new antagonists. *Mol Pharmacol*. 50:923–930.
- Compte A, Sanchez-Vives MV, McCormick DA, Wang X-J. 2003. Cellular and network mechanisms of slow oscillatory activity (<1 Hz) and wave propagations in a cortical network model. *J Neurophysiol*. 89:2707–2725.
- Steriade M, Nuñez A, Amzica F. 1993. A novel slow (<1 Hz) oscillation of neocortical neurons in vivo: depolarizing and hyperpolarizing components. *J Neurosci*. 13:3252–3265.
- Ruiz-Mejias M, Ciria-Suarez L, Mattia M, Sanchez-Vives MV. 2011. Slow and fast rhythms generated in the cerebral cortex of the anesthetized mouse. *J Neurophysiol*. 106:2910–2921.
- Camassa A, Galluzzi A, Mattia M, Sanchez-Vives MV. 2022. Deterministic and stochastic components of cortical down states: dynamics and modulation. *J Neurosci*. 42:9387–9400.
- Cruikshank JW, Brudzynski SM, McLachlan RS. 1994. Involvement of M1 muscarinic receptors in the initiation of cholinergically induced epileptic seizures in the rat brain. *Brain Res*. 643:125–129.
- Sanchez-Vives MV, et al. 2010. Inhibitory modulation of cortical up states. *J Neurophysiol*. 104:1314–1324.
- Steriade M, Amzica F, Nunez A. 1993. Cholinergic and noradrenergic modulation of the slow (approximately 0.3 Hz) oscillation in neocortical cells. *J Neurophysiol*. 70:1385–1400.
- Brown RE, Basheer R, McKenna JT, Strecker RE, McCarley RW. 2012. Control of sleep and wakefulness. *Physiol Rev*. 92:1087–1187.
- Platt B, Riedel G. 2011. The cholinergic system, EEG and sleep. *Behav Brain Res*. 221:499–504.
- Hudetz AG, Wood JD, Kampine JP. 2003. Cholinergic reversal of isoflurane anesthesia in rats as measured by cross-approximate entropy of the electroencephalogram. *Anesthesiology*. 99:1125–1131.
- Dasilva M, et al. 2021. Modulation of cortical slow oscillations and complexity across anesthesia levels. *NeuroImage*. 224:117415.
- Torao-Angosto M, Manasanch A, Mattia M, Sanchez-Vives MV. 2021. Up and down states during slow oscillations in slow-wave sleep and different levels of anesthesia. *Front Syst Neurosci*. 15:609645.
- Tort-Colet N, Capone C, Sanchez-Vives MV, Mattia M. 2021. Attractor competition enriches cortical dynamics during awakening from anesthesia. *Cell Rep*. 35:109270.
- Selyanko AA, et al. 2000. Inhibition of KCNQ1-4 potassium channels expressed in mammalian cells via M1 muscarinic acetylcholine receptors. *J Physiol*. 522:349–355.

- 34 Dalla Porta L, Barbero-Castillo A, Sanchez-Sanchez JM, Sanchez-Vives MV. 2023. M-current modulation of cortical slow oscillations: network dynamics and computational modeling. *PLoS Comput Biol*. 19:e1011246.
- 35 Groleau M, Kang JI, Huppé-Gourgues F, Vaucher E. 2015. Distribution and effects of the muscarinic receptor subtypes in the primary visual cortex. *Front Synaptic Neurosci*. 7:10.
- 36 Salgado H, et al. 2007. Muscarinic M_2 and M_1 receptors reduce GABA release by Ca^{2+} channel modulation through activation of PI_3 K/ Ca^{2+} -independent and PLC/ Ca^{2+} -dependent PKC. *J Neurophysiol*. 98:952–965.
- 37 Moran SP, et al. 2018. M_1 -positive allosteric modulators lacking agonist activity provide the optimal profile for enhancing cognition. *Neuropsychopharmacology*. 43:1763–1771.
- 38 Davis AA, Fritz JJ, Wess J, Lah JJ, Levey AI. 2010. Deletion of M_1 muscarinic acetylcholine receptors increases amyloid pathology in vitro and in vivo. *J Neurosci*. 30:4190–4196.
- 39 Fisher A. 2008. Cholinergic treatments with emphasis on M_1 muscarinic agonists as potential disease-modifying agents for Alzheimer's disease. *Neurotherapeutics*. 5:433–442.
- 40 Melancon BJ, Tarr JC, Panarese JD, Wood MR, Lindsley CW. 2013. Allosteric modulation of the M_1 muscarinic acetylcholine receptor: improving cognition and a potential treatment for schizophrenia and Alzheimer's disease. *Drug Discov Today*. 18: 1185–1199.
- 41 Gloor P, Ball G, Schaul N. 1977. Brain lesions that produce delta waves in the EEG. *Neurology*. 27:326–333.
- 42 Massimini M, et al. 2024. Sleep-like cortical dynamics during wakefulness and their network effects following brain injury. *Nat Commun*. 15:7207.
- 43 Hay YA, et al. 2021. Cholinergic modulation of Up–Down states in the mouse medial entorhinal cortex in vitro. *Eur J Neurosci*. 53: 1378–1393.
- 44 Cancino-Fuentes N, et al. 2024. Recording physiological and pathological cortical activity and exogenous electric fields using graphene microtransistor arrays in vitro. *Nanoscale*. 16:664–677.
- 45 Fisher RS. 2012. Therapeutic devices for epilepsy. *Ann Neurol*. 71: 157–168.
- 46 Kamsler A, McHugh TJ, Gerber D, Huang SY, Tonegawa S. 2010. Presynaptic m_1 muscarinic receptors are necessary for mGluR long-term depression in the hippocampus. *Proc Natl Acad Sci U S A*. 107:1618–1623.
- 47 Sheffler DJ, et al. 2009. A novel selective muscarinic acetylcholine receptor subtype 1 antagonist reduces seizures without impairing hippocampus-dependent learning. *Mol Pharmacol*. 76: 356–368.
- 48 Kienzler MA, et al. 2013. A red-shifted, fast-relaxing azobenzene photoswitch for visible light control of an ionotropic glutamate receptor. *J Am Chem Soc*. 135:17683–17686.
- 49 Izquierdo-Serra M, et al. 2014. Two-photon neuronal and astrocytic stimulation with azobenzene-based photoswitches. *J Am Chem Soc*. 136:8693–8701.
- 50 Sortino R, et al. 2023. Three-photon infrared stimulation of endogenous neuroreceptors in vivo. *Angew Chem Int Ed Engl*. 62: e202311181.
- 51 Sanchez-Vives MV. Spontaneous rhythmic activity in the adult cerebral cortex in vitro. In: Ballanyi K, editors. *Isolated central nervous system circuits neuromethods*. Humana Press, 2012. p. 263–284.
- 52 Aghajanian GK, Rasmussen K. 1989. Intracellular studies in the facial nucleus illustrating a simple new method for obtaining viable motoneurons in adult rat brain slices. *Synapse*. 3:331–338.
- 53 Mattia M, Ferraina S, Del Giudice P. 2010. Dissociated multi-unit activity and local field potentials: a theory inspired analysis of a motor decision task. *NeuroImage*. 52:812–823.
- 54 D'Andola M, et al. 2018. Bistability, causality, and complexity in cortical networks: an in vitro perturbational study. *Cereb Cortex*. 28:2233–2242.